Journal of Materials Chemistry A

Accepted Manuscript

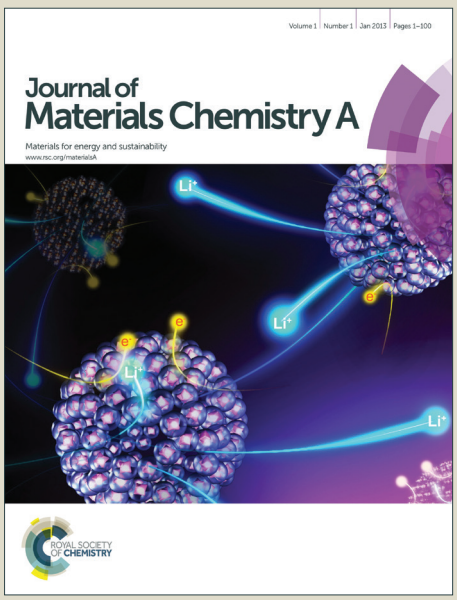

ROYAL SOCIETY OF CHEMISTRY

www.rsc.org/materialsA

Journal Name

ARTICLE

Tuning visible-light absorption properties of Ru-diacetylide complexes: a simple access to colorful efficient dyes for DSSCs

Samuel De Sousa, Siliu Lyu, Laurent Ducasse, Thierry Toupance* and Céline Olivier*

Received 00th January 20xx,
Accepted 00th January 20xx

DOI: 10.1039/x0xx00000x

www.rsc.org/

A series of σ-dialkynyl ruthenium complexes showing a D–π–[M]–π–A structure (where [M] = [Ru(dppe)2], dppe = bisdiphenylphosphinoethane) was designed and synthesized for dye-sensitized solar cells (DSSCs) applications. The molecular structure of these highly modular organometallic complexes was fine-tuned through the introduction of a bithiophene, rhodanine or benzothiadiazole unit. This original molecular engineering approach combined with convergent synthetic pathways thus afforded efficient photosensitizers with tunable colors across the visible spectrum, ranging from red to purple, blue and blue-green dyes. The optoelectronic properties of the new complexes were fully assessed and the dyes were tested in standard single-dye devices as well as in co-sensitized DSSCs, yielding 7.5 % power conversion efficiency in presence of an iodine-based liquid electrolyte.

1. Introduction

The development of efficient and all at once easy-manufacturing systems for the widespread use of photovoltaics is a highly challenging field of research for our modern societies. In this context, dye-sensitized solar cells (DSSCs) that capture light with synthetic pigments have drawn much attention over the past 25 years,[1] and showed overall energy conversion efficiencies competing with those of amorphous silicon-based solar cells.[2] In particular, the DSSC technology requires careful molecular engineering to get easy-to-make photosensitizers with high photovoltaic performance and long-term stability. In a DSSC, solar light is harvested by dye molecules covalently anchored onto a wide-bandgap semiconductor thin-film, usually TiO_2. Upon photo-excitation of the dyes, electrons rapidly transfer to the conduction band of the semiconductor. The photo-generated electrons are then transported towards the front electrode and flow into the external circuit. The oxidized dyes are then reduced back to their neutral state by a redox mediator present in the electrolyte solution, usually comprised of the iodide/triiodide couple (I^- /I_3^-) that transports positive charges to a platinized counter-electrode.[3]

A significant benefit of DSSC over almost all other kinds of technologies is that it can be constructed from abundant, non-toxic and cheap materials.[1a] Thus, commercialization of this new energy-generating device already emerged for different fields of applications. Today, key markets for DSSCs are consumer products, such as wireless self-powering stand-alone devices for indoor and outdoor utilization.[4] Nonetheless, thanks to their transparency and workability under low-light conditions, DSSCs are also particularly well suited for building-integrated photovoltaics (BIPV) where power-supplying devices replace conventional building materials such as window glass.[4,5] In this scope, to create even more aesthetic solar panels and façades, a clear need exists to diversify the range of available colors, while keeping high efficiency devices.[6] Thus, the control of simply accessible, multi-colored and efficient dyes would bring a major asset towards built-in solar energy supply.

Common dyes for DSSCs are mainly composed of either ruthenium polypyridyl coordination complexes or fully organic π-conjugated architectures, a large part of them leading to orange and red pigments.[7] However the preparation of blue or blue-green single-colored efficient dyes for DSSCs is still not straightforward,[8] and thus, strong incentive remains to find new molecular designs for this purpose. Besides, the control of multiple dyes with complementary spectral sensitivity can be valued through the co-sensitization approach, which is the combination of two or more dyes within a single device to get panchromatic visible-light absorption.[8b,9]

In a recent work we reported the first example of chromophore for DSSCs presenting a ruthenium-diacetylide moiety embodied within a push-pull structure.[10] The original D–π–[M]–π–A structural design in which [M] = [$Ru(dppe)_2$] led to an innovative organometallic sensitizer with strong light-harvesting properties and afforded 7.3 % overall solar-to-power conversion efficiency. This represents the highest efficiency reported for DSSCs comprising organometallic complexes with a metal-diacetylide backbone.[11,12] However, in that case, the

Institut des Sciences Moléculaires, UMR CNRS 5255, Université de Bordeaux, 33405 Talence Cedex, France. Tel: + 33 5 40 00 24 25.
E-mail: c.olivier@ism.u-bordeaux1.fr ; t.toupance@ism.u-bordeaux1.fr.
Electronic Supplementary Information (ESI) available: materials and methods, synthetic procedures and compounds characterization, theoretical calculations details. See DOI: 10.1039/x0xx00000x

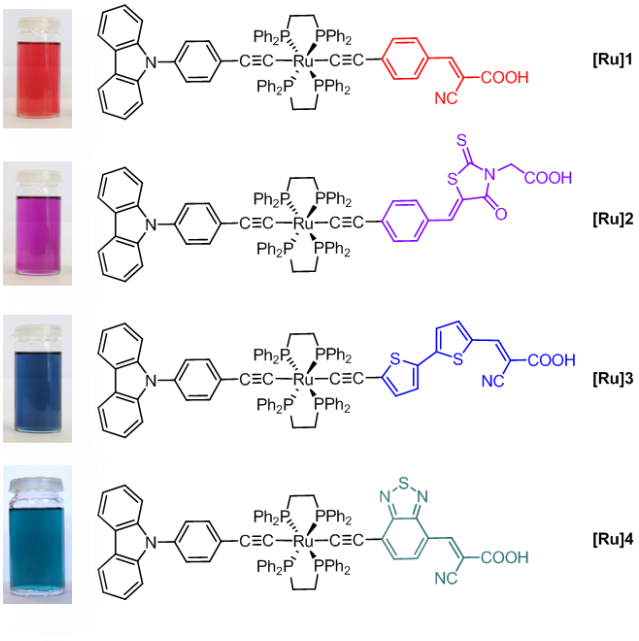

Figure 1. Molecular structure of the Ru-diacetylide complexes **[Ru]1-[Ru]4** and pictures of the new dyes in solution.

spectral absorption range of the dye was limited to short wavelengths, below 600 nm. In order to improve light absorption at higher wavelengths, and thus to obtain low band-gap dyes, we thereafter developed a simple design strategy to prepare an original series of multi-colored and efficient dyes for DSSCs. Furthermore, in the race towards panchromatic solar energy conversion, the preparation of low-band gap organic materials for photovoltaics is highly challenging.[13]

Accordingly, the implementation of simple modifications to the structure of the beforehand described complex **[Ru]1** afforded three new complexes, **[Ru]2**, **[Ru]3** and **[Ru]4**. The whole series of dyes constitutes an attractive color palette of red, violet, blue and greenish pigments (Fig. 1). All the push-pull complexes are endowed with a carbazole motif as electron-donating group and the π-conjugated linker encompasses the electron-rich [Ru(dppe)$_2$] metal fragment. Then, in accordance with the strategy widely adopted in bulk-heterojunction solar cells, which consists in using acceptors with varying electron-withdrawing ability in order to obtain narrow-band-gap small molecules,[14] the major structural difference of the new dyes lays in the acceptor part of the complexes. **[Ru]1** presents the simplest acceptor part of the series, a phenyl ring substituted by a cyanoacrylic acid anchoring group. Subsequent introduction of a rhodanine, bithiophene or benzothiadiazole motif into the molecular backbone, in order to increase the conjugation pathway as well as electron-withdrawing effect, allowed easy fine-tuning of the dyes optical properties. We herein report the optoelectronic study of the new series of dyes and an analysis of their photovoltaic performance in DSSCs.

2. Experimental Section

2.1 Materials and methods

All the details relative to the synthesis of the organic precursors and organometallic complexes are given in the Electronic Supplementary Information (ESI). UV-visible absorption and emission fluorescence spectra were recorded on a UV-1650PC SHIMADZU spectrophotometer and on a FluoroMax-4 HORIBA spectrofluorometer, respectively. Cyclic voltammetry analyses were carried out on an Autolab PGSTAT100 potentiostat/galvanostat. Measurements were performed in CH_2Cl_2 solutions including 0.1M of Bu_4NPF_6 as salt support, at scan rate of 100 mV.s^{-1}, using a three-electrode system: the working electrode was a Pt disc, the reference electrode was Ag/AgCl (calibrated with decamethylferrocene as internal reference) and the counter electrode was a Pt wire. Potentials were afterwards referred to NHE by addition of 130 mV.[15]

2.2 DSSC preparation and characterization

FTO-coated conducting glass substrates (NSG10, 10 ohm/□, thickness 3.2 mm, XOPFisica) were cleaned by using successive ultrasonic treatments in an alkaline detergent solution and in ethanol. The conducting glass substrates were afterwards treated by 40 mM $TiCl_4$ aqueous solution at 70°C for 30 min in order to create an ultra-thin TiO_2 blocking layer. The photoanodes were prepared by screen-printing method using commercially available titania pastes. TCO substrates were first coated with a transparent layer, composed of 20 nm anatase TiO_2 nanoparticles (Solaronix, Ti-Nanoxide T/SP). The screen-printing step was repeated three times to get an appropriate thickness of 10 µm. A diffusing layer, made of 250 to 400 nm TiO_2 particles (Solaronix, Ti-Nanoxide R/SP) was then deposited on top of the working electrode. The thickness of this scattering layer was of 5 µm. The photoanodes were treated by gradual heating under air at 325°C (5 min), 375°C (5 min), 450°C (15 min) and 500°C (15 min). The resulting films were further treated with 40 mM $TiCl_4$ aqueous solution at 70°C for 30 min followed by annealing at 500°C for 30 min. After cooling down to 40°C, the electrodes were immersed into 0.3 mM dye solutions in dichloromethane containing 1 mM of cheno-deoxycholic acid as co-adsorbent and de-aggregating agent. Under these conditions, the sensitization time was optimized to 16 hours in the dark. Platinized counter-electrodes were prepared by drop-casting a solution of H_2PtCl_6 (5 mM in ethanol) on FTO-glass substrates (TCO22-7, 7 ohm/□, thickness 2.2 mm, Solaronix). Thermal decomposition of the complex under air flow, at 500°C for 30 min, afforded sufficient amount of Pt nanoparticles. The photoanode and counter-electrode were assembled using a hot-melt Surlyn polymer gasket (25 µm, Dupont). The electrolyte was introduced into the cell by vacuum backfilling through a hole drilled in the counter-electrode. The device was finally sealed with Surlyn gasket and glass plate cover. The composition of the electrolyte Z960 is as follows: 0.03 M iodine, 0.05 M lithium iodide, 1.0 M 1,3-dimethylimidazolium iodide, 0.8 M 4-tert-butylpyridine and 0.1 M guanidinium thiocyanate in acetonitrile/valeronitrile 85:15. Photovoltaic performance of the DSSCs were measured by using a black mask with an aperture area of 0.159 cm^2. The device was illuminated by

AM1.5G solar simulator calibrated with a radiometer (IL 1400BL) to provide an incident irradiance of 100 mW cm^{-2} at the surface of the solar cells. The J-V measurements were performed using a Keithley model 2400 digital source meter by applying independently external voltage to the cell and by measuring the photo-generated current out from the cell. Action spectra of incident photon-to-current conversion efficiency (IPCE) were realized using a Xe lamp associated with a monochromator (Triax 180, Jobin Yvon) to select and increment wavelength irradiation to the cell. No bias light was employed to illuminate the cell. The current produced was measured by steps of 5 nm after 2 s of radiation exposure with a Keithley 6487 picoammeter in order to be in steady state conditions. The incident photon flux was measured with a 6-in. diameter calibrated integrated sphere and a silicon detector.

2.3 Computational methods

DFT and TD-DFT calculations were performed with Gaussian09.[16] B3LYP/LANL2DZ optimized geometies in vacuo conditions were used to perform TD-DFT calculations using the LANL2DZ basis set together with the MPW1K XC functional containing 42.8% of HF exchange,[17] while taking into account the solvent within the integral equation formalism of the polarizable continuum model (IEF-PCM).[18] This method already provided UV-vis absorption spectra of push-pull molecules in agreement with experimental data.[19] The electronic parameters describing the charge transfer (CT) processes occurring upon photoexcitation of push–pull systems were calculated by applying previously described computational methods.[20]

3. Results and discussion

3.1 Synthesis and characterization

The synthesis routes towards the dissymmetric Ru-diacetylide complexes **[Ru]1-[Ru]4** are summarized in Scheme 1. In a first step, reaction of the 16-electron species $[RuCl(dppe)_2][TfO]$ (**[1][TfO]**) with *N*-(4-ethynylphenyl)-carbazole (**2**) led to the stable ruthenium-vinylidene moiety (**[3][TfO]**),[10] which constitutes the electron-donor part of the target push-pull dyes. Subsequent reaction of **[3][TfO]** with appropriate ethynyl-aryl derivatives, in the presence of triethylamine and sodium hexafluorophosphate, allowed the formation of bis(σ-arylacetylide) intermediate complexes. Direct introduction of an alkynyl ligand bearing the cyanoacrylic acid function was hampered by coordination of the nitrile group to the ruthenium core of the vinylidene moiety **[3][TfO]**. Thus, in the synthesis route to **[Ru]1**, **[Ru]3** and **[Ru]4**, the ethynyl-substituted aryl derivatives employed to form the intermediate complexes **4a-c** were bearing a carbaldehyde function, allowing subsequent introduction of the cyanoacrylic acid group through Knoevenagel condensation. However, in order to avoid side reactions with the metal-complexes during the condensation step, protection of the carboxylic acid function was necessary. Therefore, cyanoacetic acid endowed with a silyl-ester protecting group, i. e. 2-(trimethylsilyl)ethyl (TMSE), was prepared and used. Protection by the TMSE group was preferably chosen as it allows subsequent deprotection under mild conditions, which is more appropriate to organometallic complexes. On the other hand, in the synthesis route to **[Ru]2**,

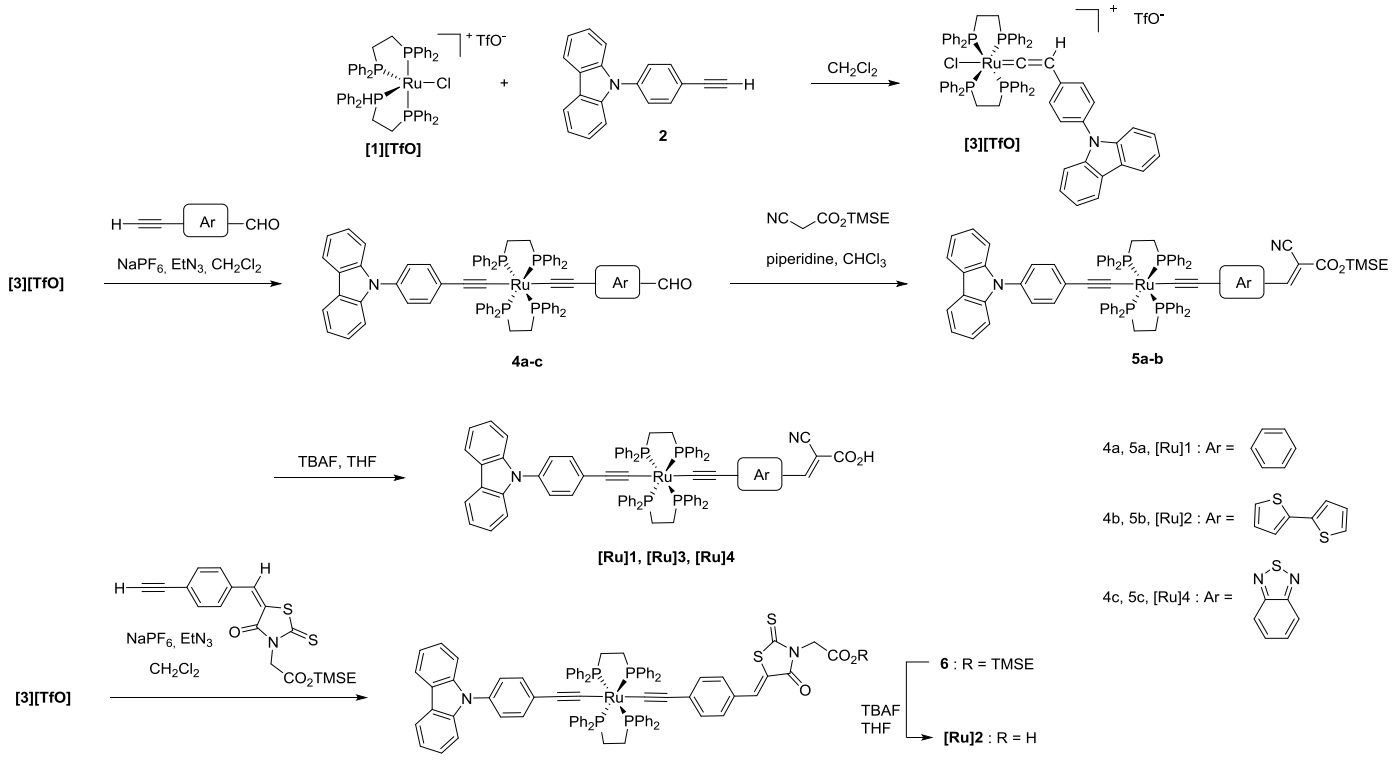

Scheme 1. Synthesis routes to **[Ru]1-[Ru]4**. TMSE = 2-(trimethylsilyl)ethyl. TBAF = tetrabutylammonium fluoride.

reaction of a TMSE-protected ethynyl-rhodanine acetic acid derivative with **[3][TfO]** was directly feasible, thus saving one reaction step compared to the cyanoacrylic acid derivatives. In the final step, silyl-ester deprotection at room temperature using tetrabutylammonium fluoride (TBAF) in THF, afforded the functionalized Ru-diacetylide complexes **[Ru]1-[Ru]4** in good yields. The new dyes and all the intermediate compounds were fully characterized by means of ^{31}P, ^{1}H and ^{13}C NMR, HR-MS and FT-IR (see ESI). All the data are in total accordance with the expected structure of the new organometallic complexes. In particular, the ^{31}P NMR spectra of the target dyes **[Ru]1-[Ru]4** exhibit a sharp singlet at *c.a.* 53-55 ppm, characteristic of the *trans*-ditopic geometry of the ruthenium-diacetylide unit. The FT-IR spectra of the four new dyes show an intense band at *c.a.* 2040 cm^{-1} for the $\nu_{C\equiv C}$ vibrational stretch of the σ-diacetylide metal fragment. In addition, characteristic peaks for the cyanoacrylic acid function were observed for **[Ru]1**, **[Ru]3** and **[Ru]4**, around 2215 cm^{-1} for the $\nu_{C\equiv N}$, and around 1710 and 1200 cm^{-1} for the $\nu_{C=O}$ and ν_{C-O} stretches, respectively. Similarly, typical vibrational stretches were observed for the carboxylic acid function of **[Ru]2** ($\nu_{C=O}$ at 1712 cm^{-1} and ν_{C-O} at 1173 cm^{-1}).

3.2 Optoelectronic properties

Electronic absorption spectra of the dyes **[Ru]1-[Ru]4** recorded in dichloromethane solutions are shown in Fig. 2 and the corresponding data are gathered in Table 1. The four dyes exhibit intense absorption bands in the 300-400 nm range. These high-energy bands stem from multiple electronic transitions involving deep molecular orbitals with important contribution of the diphosphine ligands as discussed below (see TD-DFT calculations). More interestingly, the absorption spectra of **[Ru]1-[Ru]4** show an intense band in the visible-light region with maximum wavelength ranging from λ_{max} = 521 nm for the red pigment **[Ru]1** to λ_{max} = 659 nm for the blue-green dye **[Ru]4**, with intermediate values of λ_{max} = 550 nm and λ_{max} = 608 nm for the violet and blue dyes **[Ru]2** and **[Ru]3**, respectively. Such color palette is due to significant difference in the energy of the main transition occurring within the Ru-diacetylide complexes. The broad absorption bands observed in the visible range for functionalized di-alkynyl Ru-complexes are mainly attributable to the HOMO→LUMO transition.[10,12,21] Since the HOMO level of such organometallic complexes show important contribution of the [Ru(dppe$_2$)] metal fragment (*vide infra*), the main photoinduced electronic transition presents a strong metal-to-ligand charge transfer (MLCT) character. In this study, the difference in energy observed for the main transition of the four complexes is directly related to the nature of the π-linker and of the electron-withdrawing group (EWG) on the acceptor part of the dyes. For example, replacing the cyanoacrylic acid motif in **[Ru]1** by the rhodanine acetic acid anchoring group in **[Ru]2** led to 36 nm red-shift of the maximum absorption wavelength, leading to the purple colored **[Ru]2** pigment**.** Such red shifting of the absorption maximum, due to extended π-conjugation of the system through the 4-oxo-2-thioxothiazolidine ring, is consistent with other reports comparing the cyanoacrylic acid and rhodanine acetic acid

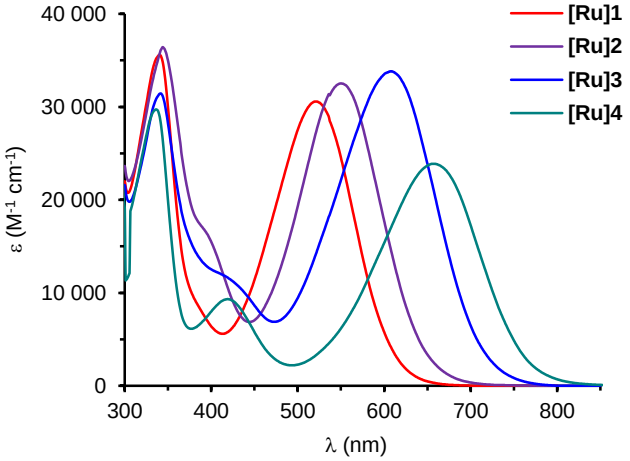

Figure 2. Absorption spectra of **[Ru]1-[Ru]4** in solution in CH_2Cl_2.

EWG.[22] Likewise, the introduction of a bithiophene unit (**[Ru]3**) in place of the benzyl ring (**[Ru]1**) led to an even more significant increase of the delocalization pathway,[11c,23] thus shifting the λ_{max} of 87 nm towards red absorptions and providing the blue colored pigment **[Ru]3**. On the other hand, the introduction of the strong acceptor benzothiadiazole into the π-conjugated linker both increased the electronic delocalization and the withdrawing effect, leading to 138 nm red-shifted absorption for **[Ru]4** compared to **[Ru]1**. Overall, as estimated from both absorption and emission spectra, the difference in visible-light absorption properties on the series is due to a decrease of the optical band-gap energy (ΔE_{opt}) in the order **[Ru]1**>**[Ru]2**>**[Ru]3**>**[Ru]4** (Table 1). In addition, except from **[Ru]4** which absorption spectrum shows slightly lower intensity compared the other complexes, the extinction coefficient of the dyes in the visible region is exceeding 30 000 $M^{-1}.cm^{-1}$, reaching

Table 1. Optical and electrochemical properties.

Dye	λ_{abs} [a]/nm ($\varepsilon/M^{-1}.cm^{-1}$)	λ_{em} [b] /nm	λ_{abs} [c] /nm	E_{ox} [d] /V	ΔE_{opt} [d] /V	$E_{ox} - \Delta E_{opt}$ [f]/V
[Ru]1	340 (35 600) 521 (30 600)	820	470	0.73	2.10	-1.37
[Ru]2	344 (36 400) 390 (sh.) 550 (32 500)	826	532	0.68	1.96	-1.28
[Ru]3	341 (31 400) 425 (sh.) 608 (33 800)	823	535	0.62	1.80	-1.18
[Ru]4	336 (29 700) 422 (9 300) 659 (23 900)	825	600	0.75	1.70	-0.95

[a] Absorption maxima in CH_2Cl_2 solution (C = 3 x 10^{-5} M). [b] Emission maximum in CH_2Cl_2 solution (C = 3 x 10^{-5} M). [c] Absorption maximum on 3µm-thick transparent TiO_2 film (dye bath containing 1mM of cheno-deoxycholic acid). [d] Oxidation potential in CH_2Cl_2 solution with $FeCp^*_2$ as internal reference. Potentials referred to NHE by addition of 130 mV.[13] [e] ΔE_{opt} estimated from the intercept of the normalized absorption and emission spectra (considering that ΔE_{opt} (V) = ΔE_{opt} (eV) / q = ΔE_{opt} (eV) / 1 = ΔE_{opt} (eV)).

up to 33 800 $M^{-1}.cm^{-1}$ for **[Ru]3**. All these features confirm the strong light-harvesting properties of Ru-diacetylide complexes as well as their great potential for the sensitization of TiO_2 and DSSC device effectiveness.

A blue-shift of the maximum absorption in the visible range was observed upon grafting the dyes onto TiO_2 transparent thin-film (Table 1, Fig. S1). The origin of the hypsochromic shift is attributable to the deprotonation of the carboxylic acid function of the dyes and to their interaction with the metal oxide surface.[19] We recently demonstrated that strong interaction exists between dye molecules and TiO_2 through the cyanoacrylic acid anchor, thus leading to significant contribution of the surface to the ground-state energy of the system and therefore to a higher energy of the main photoinduced transition.[24] The blue-shift in the range of 50-70 nm observed for **[Ru]1**, **[Ru]3** and **[Ru]4** upon chemisorption is consistent with that reported for organic push-pull dyes bearing the cyanoacrylic acid anchoring function.[24,25] On the other hand, due the conjugation breaking by the methylene swivel, the electronic coupling of **[Ru]2** with TiO_2 through the rhodanine acetic acid group appeared to be weaker and therefore the observed blue-shift was smaller than for the three other dyes (18 nm). Nonetheless, the main absorption band of the dye-sensitized TiO_2 films remained broad in the visible region, with high optical density, and the hypsochromic effect resulting from surface-anchoring of the dyes did not preclude their light-harvesting properties.

3.3 Electrochemical properties

The redox properties of the complexes **[Ru]1-[Ru]4** were investigated through cyclic voltammetry analyses performed in CH_2Cl_2 solutions including Bu_4NPF_6 as salt support (Table 1). Upon oxidation, the voltammograms showed one reversible monoelectronic process corresponding to the first oxidation potential of the dyes (E_{ox}) and one irreversible process at higher potential indicating chemical instability of the second oxidized species. Compared to **[Ru]1**, the electronic enrichment of the π-conjugated system through introduction of a rhodanine or a bithiophene unit in **[Ru]2** and **[Ru]3**, respectively, led to significant decrease of the first oxidation potential ($E_{ox([Ru]1)}$ = + 0.73 V ; $E_{ox([Ru]2)}$ = + 0.68 V ; $E_{ox([Ru]3)}$ = + 0.62 V *vs* NHE). Conversely, the introduction of the benzothiadiazole acceptor moiety in **[Ru]4** led to slightly more positive oxidation process ($E_{ox([Ru]4)}$ = + 0.75 V *vs* NHE). Nonetheless, the first oxidation potential of the four complexes **[Ru]1-[Ru]4** stands sufficiently higher than the standard potential of I_3^-/I^- (E^0 = + 0.45 V *vs* NHE) to guarantee efficient regeneration of the dyes by this redox mediator in DSSC devices. Combined analyses of the optical and electrochemical data further allowed to estimate the position of the dyes LUMO energy level. The later was determined from the difference between the HOMO level, assimilated to the first oxidation potential (E_{ox}), and the optical-band gap (ΔE_{opt}), estimated from the intercept of the normalized absorption and emission spectra of the dyes. As expected, the calculated LUMO levels (E_{ox}-ΔE_{opt}) also rely heavily on the nature of the π-linker and EWG on the acceptor part of the molecule. While the rhodanine and bithiophene units induced stabilization of the LUMO by 90 mV and 190 mV for **[Ru]2** and **[Ru]3**, respectively, compared to **[Ru]1** (E_{ox}-$\Delta E_{opt([Ru]1)}$ = - 1.37 V ; E_{ox}-$\Delta E_{opt([Ru]2)}$ = - 1.28 V ; E_{ox}-$\Delta E_{opt([Ru]3)}$ = - 1.18 V), the much stronger electron-withdrawing effect proceeding in **[Ru]4**, thanks to the benzothiadiazole, led to the lowest LUMO level of the series (E_{ox}-$\Delta E_{opt([Ru]4)}$ = - 0.95 V). This one is stabilized by 420 mV compared to **[Ru]1**. However, the experimentally estimated LUMO levels of the four dyes remain more negative than the conduction band edge of TiO_2 (*ca.* - 0.50 V *vs* NHE) indicating that efficient electron transfer should occur from the photoexcited dyes to the semi-conducting oxide.

3.4 Theoretical calculations

Quantum chemical calculations were carried out in order to gain deeper insights into the molecular orbital (MO) distribution and the electronic transitions occurring upon photoexcitation of the dyes **[Ru]1-[Ru]4**. Optimized geometry of the complexes were obtained from density functional theory (DFT) at the B3LYP/6-31g(d) level in vacuo. Time-dependent density functional theory (TD-DFT) calculations, performed using the standard 6-31g(d)

Table 2. Theoretical data of the lowest energy allowed transitions.

Dye	ΔE_{ge} /eV [a]	λ_{ge} /nm [b]	f_{ge} [c]	Transition assignment (coefficient) [d]	Λ [e]	q_{CT} / e [f]	D_{CT} / Å [g]
[Ru]1	2.636	470	1.044	**H→L (0.64)**; H-2→L (-0.21)	0.46	1.08	4.6
	4.136	300	0.911	H→L+1 (0.15); H→L+3 (0.38); H→L+4 (0.43)			
[Ru]2	2.500	496	1.339	**H→L (0.63)**; H-1→L (-0.18); H-2→L (-0.18)	0.43	1.10	5.0
	4.020	308	0.593	H-1→L+1 (-0.19); H→L+1 (0.53); H→L+4 (-0.18); H→L+5 (-0.19)			
[Ru]3	2.138	580	1.733	**H→L (0.64)**; H-1→L (0.23)	0.60	0.87	4.8
	4.140	299	0.864	H-1→L+1 (-0.21); H-1→L+4 (-0.21); H-1→L+5 (-0.20); H→L+4 (0.37); H→L+5 (0.30)			
[Ru]4	1.928	643	0.861	**H→L (0.64)**; H-2→L (-0.27)	0.55	0.88	3.8
	3.166	391	0.106	**H→L+1 (0.51)**; H-1→L+1 (0.21); H-2→L+1 (-0.20)			
	4.183	296	0.945	H→L+3 (-0.17); H→L+4 (0.54)			

[a] ΔE_{ge} = main transition energy. [b] λ_{ge} = calculated λ_{max}. [c] f_{ge} = oscillator strength. [d] Only the transitions with coefficients higher than 0.15 are given. [e] Λ = spatial overlap. [f] q_{CT} = quantity of transferred charge. [g] D_{CT} = distance between the barycentres of the density depletion and density increment zones related to the CT excitation.

provided information about the main transitions energy and related oscillator strengths. The corresponding data are listed in Table 2. The layout of simulated absorption spectra (see Fig. S2) is in very good agreement with the experimental one. Two main absorption bands are observed, one around 300 nm and one in the visible region. A third absorption band appears around 400 nm for **[Ru]4**. The order of the calculated maximum wavelengths in the visible part perfectly matches the experimental data, λ**[Ru]1** < λ**[Ru]2** < λ**[Ru]3** < λ**[Ru]4**. The small deviation between the calculated and experimental data is due to the large size of the organometallic complexes.

Theoretical calculations also allowed assignment, as well as representation, of the main transition-involved molecular orbitals. The computed data in Table 2 confirmed that, uniformly for the four dyes, the lowest energy transition owns a major HOMO→LUMO character. At the ground-state the electronic density of the HOMO is highly delocalized over the whole π-conjugated system with sizeable contribution of the –C≡C–[Ru]–C≡C– fragment. Conversely, at the excited-state, the electronic density, through transfer to the LUMO, is pulled towards the cyanoacrylic acid or rhodanine acetic acid EWG and therefore close to TiO_2 surface. From the isodensity plots of the deeper MOs, we could infer that the additional electronic transitions contributing to the dyes response in the visible region (i.e. HOMO-1→LUMO, HOMO-2→LUMO) are fairly similar to the HOMO→LUMO transition. Thus, as expected for these organometallic complexes, the large absorption band in the visible range presents a strong MLCT character. Assignment of the intense absorption bands at lower wavelengths revealed that multiple electronic transitions also occur in this region, involving high energy orbitals such as LUMO+1, LUMO+3, LUMO+4, LUMO+5. The latter are mostly localized on the [Ru(dppe)$_2$] fragment with strong contribution of the diphosphine ligands. Each transition is illustrated in the ESI (Fig. S3a-i). In addition, the calculated energy diagram of the dyes' main transition-involved MOs is represented in Fig. S4. It appears that, except from **[Ru]4** which is slightly destabilized, the HOMO levels of the dyes are very close in energy, whereas the calculated LUMO energy levels decrease significantly in the order **[Ru]1** > **[Ru]2** > **[Ru]3** > **[Ru]4**. This is perfectly consistent with the experimental data (Table 1). Moreover, an important energy gap exists between the LUMO and LUMO+1 orbitals of **[Ru]1**, **[Ru]2** and **[Ru]3** (~ 1.3 eV), whereas in **[Ru]4** the LUMO+1 is strongly stabilized leading to a smaller gap of 1.0 eV. This resulted in an additional absorption band for **[Ru]4**, as observed both on the experimental and calculated absorption spectra. This transition occurring at intermediate energy owns a major HOMO→LUMO+1 character. From Fig. S3.h we could infer that, due to the strong withdrawing effect of the benzothiadiazole motif, the LUMO+1 in **[Ru]4** is unlike in the three other dyes. Likewise the LUMO, the LUMO+1 of **[Ru]4** is fully located on the acceptor part of the molecule, thus enabling the observed extra absorption band (see also Table S1).

The parameters characterizing the photo-induced charge transfer processes occurring in push–pull systems were calculated using recently described computational methods (see Table 2).[18] The calculated amount of transferred charge (q_{CT}) is close to 1 for all dyes meaning that the visible-range electronic transition occurring within the complexes shows a net charge-transfer character and proceeds in a highly efficient way. It is also worth to note that the calculated charge-transfer distances (D_{CT}) are following the same trend as the distance between the electron rich metal fragment [Ru(dppe)$_2$] and the EWG (cyanoacrylic acid in **[Ru]1-[Ru]3**, rhodanine in **[Ru]2** and benzothiadiazole in **[Ru]4**).

3.5 Photovoltaic characterization

The photovoltaic performances of **[Ru]1-[Ru]4** in DSSCs were assessed under standard conditions, i. e. simulated AM 1.5G illumination (100 mW.cm-2) using an iodine-iodide liquid electrolyte (see Experimental Section for details). Characteristic photocurrent density/voltage (J/V) curves and incident photon-to-current conversion efficiency (IPCE) spectra are presented in Fig. 3. The corresponding photovoltaic parameters (J_{SC} : short-circuit current density; V_{OC} : open-circuit voltage, *ff* : fill factor; η : overall power conversion efficiency) are listed in Table 3. Additionally, the amount of adsorbed dye molecules on TiO_2 electrodes was assessed by spectroscopic methods, the results are reported in Table 3.

Analysis of the J/V curves indicates that **[Ru]1** and **[Ru]3** yielded comparable overall power conversion efficiency (7.32 % and 7.08 % PCE, respectively) while **[Ru]2** and **[Ru]4** both afforded 6.10 % PCE. Due to advantageous light-harvesting properties, the dye **[Ru]3** showed the highest short-circuit current density of the series (J_{SC} = 17.15 mA.cm^{-2}), although lower open-circuit voltage (V_{OC} = 610 mV V) compared to **[Ru]1** (V_{OC} = 679 mV). However, it is worth to note that the overall performance obtained with **[Ru]3** is among the best reported for blue sensitizers in the presence of an iodine-based liquid electrolyte. Indeed the maximum PCE reported for a squaraine-sensitized DSSC is of 7.3 %,[26] and 7.1-7.7 % PCE was recently achieved using a series of blue-colored dyes implementing the deketopyrrolopyrrole motif.[27]

Table 3. Photovoltaic performance [a] of DSSCs based on **[Ru]1-[Ru]4** and dye loadings on TiO_2.

Dye	J_{SC} (mA.cm^{-2})	V_{OC} (mV)	*ff* (%)	η (%)	*Amount* [b] (mol.cm^{-2})
[Ru]1	15.56	679	69.2	7.32	2.80 x 10^{-7}
[Ru]2	14.82	610	67.5	6.11	2.40 x 10^{-7}
[Ru]3	17.15	608	68.0	7.08	2.92 x 10^{-7}
[Ru]4	16.23	582	64.7	6.10	2.66 x 10^{-7}
[Ru]1&[Ru]3	15.70	650	73.4	7.49	2.82 x 10^{-7}

[a] Photovoltaic data measured at full sunlight (AM 1.5G, 100 mW cm^{-2}); TiO_2 film thickness = 10 µm (transparent) + 5 µm (scattering); active area = 0.159 cm^2.[28] Data from the best of six devices (standard deviation on the efficiency ± 0.05 %). [b] Dye loading amount measured on 1 cm^2 TiO_2 electrodes.

Interestingly, likewise typically observed with porphyrins, phthalocyanines and fully organic sensitizers, the dyes **[Ru]1-[Ru]4** show poorer V_{OC} than benchmark ruthenium dyes such as N719 or N3.[28] This characteristic feature of highly conjugated push-pull dyes, was attributed to shorter electron lifetime

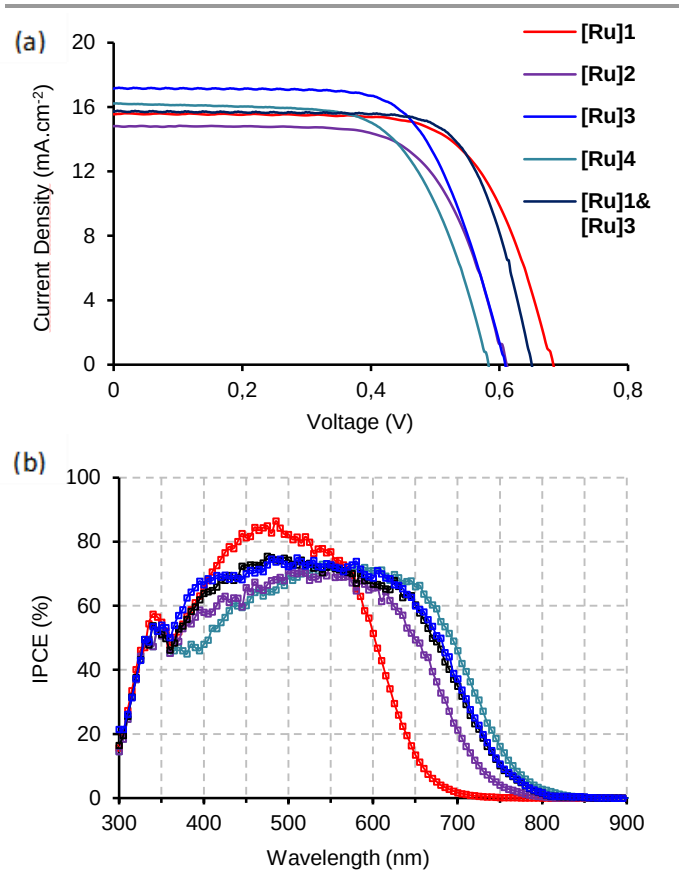

Figure 3. (a) J/V characteristics and (b) IPCE spectra of **[Ru]1**-**[Ru]4** and of **[Ru]1&[Ru]3** in DSSC.

originating from fast recombination reactions between injected electrons in the TiO_2 electrode and the electrolyte,[29] i. e. higher dark current due to poorer coverage of the surface by linear D-π-A systems rather than bulky complexes.

Despite good absorption properties, **[Ru]2** afforded lower short-circuit current density than the three other dyes. This can be related to electronic conjugation disruption across the rhodanine acetic acid anchoring group, leading to lower overlap between the electron density of the dye's LUMO and the semi-conductor surface, thus hampering fast electron injection.[30] Moreover the tilt angle engendered by the acetic acid motif induces unfavorable orientation of the dye on the surface of TiO_2 that facilitates electron recombination processes, thus affecting both the current density and the photovoltage.[31] In addition, the lower J_{SC} of **[Ru]2** is consistent with the slightly smaller amount of dye on TiO_2 (Table 3), the dye-loading being limited by the tilted orientation of the molecules on the metal-oxide surface.

Although yielding good photocurrent (J_{SC} = 16.23 mA.cm^{-2}), **[Ru]4** afforded the lowest open-circuit voltage of the series (V_{OC} = 582 V). This feature results from the proximity of the dye anchoring function with the benzothiadiazole EWG. The strong acceptor, when located too close to the semiconductor surface, at once favors back electron transfers from TiO_2 to the oxidized dye, and also induces a downward shift of the titania conduction band edge thus leading to low V_{OC} values.[2b,32]

The global layout of the IPCE profiles shown in Fig. 3b is in good agreement with the dyes UV-visible absorption spectra. Overall, the IPCE curves are broad with a large plateau in the visible region, which is correlated to the high extinction coefficient (Fig. 2, Table 1) and to the amount of dye-loading on TiO_2 films (Table 3). Likewise the tendency observed for the maximum absorption wavelengths, the action spectra show enhanced red response in the order **[Ru]2** > **[Ru]3** > **[Ru]4**, compared to **[Ru]1**. The IPCE of **[Ru]3** and **[Ru]4** therefore covers the visible region entirely, the onset of the curves extending beyond 800 nm.

As illustrated in Fig. S5, the two most-efficient dyes, **[Ru]1** and **[Ru]3**, show complementary spectral response, thus providing panchromatic visible-light harvesting capacity for the mixture of both in solution. This attractive feature prompted us to combine the two sensitizers in the same DSSC device through co-sensitization technique. Optimization of the photoanode staining conditions eventually led to slightly improved PCE with respect to the single-dye devices, the **[Ru]1&[Ru]3** mixture in a 4:1 molar ratio yielding up to 7.5 % PCE. As observed on the IPCE profile (Fig. 3b, S6), the use of **[Ru]3** as additional NIR-absorbing co-sensitization dye substantially improved the device red response compared to **[Ru]1** alone. However, the J_{SC} value of 15.70 mA.cm^{-2} obtained with the co-sensitized device is comparable to that of **[Ru1]**-based single-dye device, and the outcoming V_{OC} is averaged. Hence, further optimization is needed for the co-sensitization technique, which is currently under thorough investigations to increase the overall device efficiency.

Conclusions

In summary, a series of ruthenium-diacetylide complexes showing push-pull structure and appropriate functional anchoring groups were prepared for dye-sensitized solar cells applications. Simple modification of the alkynyl ligand on the acceptor side afforded a nice color palette of visible-light absorbers, ranging from red (**[Ru]1**) to purple (**[Ru]2**) and blue-green dyes (**[Ru]3**-**[Ru]4**). Spectroscopic and electrochemical studies of the complexes confirmed suitable opto-electronic properties for use in DSSC devices. In single-dye devices, the best photovoltaic performance of the series was obtained with the red dye **[Ru]1**, 7.32 % PCE, and the performance achieved by the blue dye **[Ru]3** was very close, 7.08 % PCE, which places it among the best blue-colored dyes for DSSCs. The spectral complementarity of these two dyes prompted us to test them in co-sensitized conditions which afforded slightly improved performance with regard to single-dye devices, i. e. 7.49 % PCE. Both the molecular structure of the Ru-diacetylide dyes and the co-sensitization approach are still under thorough investigations to further improve the performance of DSSCs based on these highly versatile complexes.

Acknowledgements

This work was supported by the CNRS and Région Aquitaine (Ph.D grant to SD), the China Scholarship Council (Ph.D. grant to

SL) and the ANR (CORuS project, ANR-14-CE05-0013). The authors also thank Dr L. Hirsch for help with photovoltaic characterization.

Notes and references

1 (a) B. O'Regan and M. Grätzel, *Nature*, 1991, **353**, 737. (b) M. Grätzel, *J. Photochem. Photobiol. C: Photochem. Rev.*, 2003, **4**, 14. (c) A. Hagfeldt, G. Boschloo, L. Sun, L. Kloo and H. Pettersson, *Chem. Rev.,* 2010, **110**, 6595.

2 (a) S. Mathew, A. Yella, P. Gao, R. Humphry-Baker, B. F. E. Curchod, N. Ashari-Astani, I. Tavernelli, U. Rothlisberger, Md. K. Nazeeruddin and M. Grätzel, *Nature Chem.,* 2014, **6***,* 242. (b) A. Yella, C.-L. Mai, S. M. Zakeeruddin, S.-N. Chang, C.-H. Hsieh, C.-Y. Yeh and M. Grätzel, *Angew. Chem. Int. Ed*., 2014, **53**, 2973. (c) Z. Yao, M. Zhang, R. Li, L. Yang, Y. Qiao, and P. Wang, *Angew. Chem. Int. Ed*., 2015, **54**, 5994.

3 M. Grätzel, *Nature*, 2001, **414**, 338.

4 A. Fakharuddin, R. Jose, T. M. Brown, F. Fabregat-Santiago and J. Bisquert, *Energy Environ. Sci.*, 2014, **7**, 3952.

5 (a) S. Yoon, S. Tak, J. Kim, Y. Jun, K. Kang and J. Park, *Building Environ.*, 2011, **46**, 1899. (b) A. Reale, L. Cinà, A. Malatesta, R. De Marco, T. M. Brown and A. Di Carlo, *Energy Technol.*, 2014, **2**, 531. (c) C. Cornaro, S. Bartocci, D. Musella, C. Strati, A. Lanuti, S. Mastroianni, S. Penna, A. Guidobaldi, F. Giordano, E. Patrolati, T. M. Brown, A. Reale, and A. Di Carlo, *Prog. Photovolt: Res. Appl.*, 2015, **23**, 215.

6 W. Zhang, M. Anaya, G. Lorano, M. E. Calvo, M. B. Johnston, H. Míguez and H. J. Snaith, *Nano Lett.*, 2015, **15**, 1698.

7 (a) J.-F. Yina, M. Velayudhama, D. Bhattacharyaa, H.-C. Linb and K.-L. Lua, *Coord. Chem. Rev.*, 2012, **256**, 3008. (b) Y. Wu and W. Zhu, *Chem. Soc. Rev.*, 2013, **42**, 2039. (c) M. Liang and J. Chen, *Chem. Soc. Rev.*, 2013, **42**, 3453.

8 (a) S. Zhang, X. Yang, Y. Numata and L. Han, *Energy Environ. Sci.*, 2013, **6**, 1443. (b) C.-P. Lee, R. Y.-Y. Lin, L.-Y. Lin, C.-T. Li, T.-C. Chu, S.-S. Sun, J. T. Lin and K.-C. Ho, *RSC Adv.*, 2015, **5**, 23810.

9 J.-H. Yum, E. Baranoff, S. Wenger, M. K. Nazeeruddin and M. Grätzel, *Energy Environ. Sci.*, 2011, **4**, 842.

10 S. De Sousa, L. Ducasse, B. Kauffmann, T. Toupance and C. Olivier, *Chem. Eur. J.*, 2014, **20**, 7017.

11 (a) W. Wu, X. Xu, H. Yang, J. Hua, X. Zhang, L. Zhang, Y. Long and H. Tian, *J. Mater. Chem.,* 2011, **21**, 10666. (b) W. Wu, J. Zhang, H. Yang, B. Jin, Y. Hue, J. Hua, C. Jing, Y. Long and H. Tian, *J. Mater. Chem.,* 2012, **22**, 5382. (c) S. Gauthier, B. Caro, F. Robin-Le Guen, N. Bhuvanesh, J. A. Gladysz, L. Wojcik, N. Le Poul, A. Planchat, Y. Pellegrin E. Blart, D. Jacquemin and F. Odobel, *Dalton Trans.*, 2014, **43**, 11233.

12 F. Nisic, A. Colombo, C. Dragonetti, E. Garoni, D. Marinotto, S. Righetto, F. De Angelis, M. G. Lobello, P. Salvatori, P. Biagini and F. Melchiorre, *Organometallics*, 2015, **34**, 94.

13 (a) L. Dou, J. Gao, E. Richard, J. You, C.-C. Chen, K. C. Cha, Y. He, G. Li and Y. Yang, *J. Am. Chem. Soc.*, 2012, **134**, 10071. (b) W. Yue, X. Huang, J. Yuan, W. Ma, F. C. Krebs and D. Yu, *J. Mater. Chem. A*, 2013, **1**, 10116.

14 (a) J. Yuan, Z. Zhai, J. Li, J. Lu, X. Huang, Z. Xu and W. Ma, *J. Mater. Chem. A*, 2013, **1**, 12128. (b) J. Yuan, A. Gallagher, Z. Liu, Y. Sun and W. Ma, *J. Mater. Chem. A*, 2015, **3**, 2572.

15 J. Ruiz Aranzaes, M.-C. Daniel and D. Astruc, *Can. J. Chem.*, 2013, **84**, 288.

16 Gaussian 09, Revision A.02, M. J. Frisch, G. W. Trucks, H. B. Schlegel, G. E. Scuseria, M. A. Robb, J. R. Cheeseman, G. Scalmani, V. Barone, B. Mennucci, G. A. Petersson, H. Nakatsuji, M. Caricato, X. Li, H. P. Hratchian, A. F. Izmaylov, J. Bloino, G. Zheng, J. L. Sonnenberg, M. Hada, M. Ehara, K. Toyota, R. Fukuda, J. Hasegawa, M. Ishida, T. Nakajima, Y. Honda, O. Kitao, H. Nakai, T. Vreven, J. A. Montgomery, Jr., J. E. Peralta, F. Ogliaro, M. Bearpark, J. J. Heyd, E. Brothers, K. N. Kudin, V. N. Staroverov, R. Kobayashi, J. Normand, K. Raghavachari, A. Rendell, J. C. Burant, S. S. Iyengar, J. Tomasi, M. Cossi, N. Rega, J. M. Millam, M. Klene, J. E. Knox, J. B. Cross, V. Bakken, C. Adamo, J. Jaramillo, R. Gomperts, R. E. Stratmann, O. Yazyev, A. J. Austin, R. Cammi, C. Pomelli, J. W. Ochterski, R. L. Martin, K. Morokuma, V. G. Zakrzewski, G. A. Voth, P. Salvador, J. J. Dannenberg, S. Dapprich, A. D. Daniels, Ö. Farkas, J. B. Foresman, J. V. Ortiz, J. Cioslowski and D. J. Fox, Gaussian, Inc., Wallingford CT, 2009.

17 B. J. Lynch, P. L. Fast, M. Harris and D. G. Truhlar, *J. Phys. Chem. A*, 2000, **104**, 4811.

18 (a) J. Tomasi and M. Persico, *Chem. Rev.*, 1994, **94**, 2027. (b) J. Tomasi, B. Mennucci and R. Cammi, *Chem. Rev.*, 2005, **105**, 2999.

19 L. Ducasse, F. Castet, R. Méreau, S. Nénon, J. Idé, T. Toupance and C. Olivier*, Chem. Phys. Lett.*, 2013, **556**, 151.

20 (a) M. J. G. Peach, P. Benfield, T. Helgaker and D. J. Tozer, *J. Chem. Phys.*, 2008, **128**, 044118. (b) T. Le Bahers, C. Adamo and I. Ciofini, *J. Chem. Theory Comput.*, 2011, **7**, 2498. (c) D. Jacquemin, T. Le Bahers, C. Adamo and I. Ciofini, *Phys. Chem. Chem. Phys.*, 2012, **14**, 5383.

21 F. Meng, Y.-M. Hervault, L. Norel, K. Costuas, C. Van Dyck, V. Geskin, J. Cornil, H. H. Hng, S. Rigaut and X. Chen, *Chem. Sci.*, 2012, **3**, 3113.

22 (a) H. Tian, X. Yang, R. Chen, Y. Pan, L. Li, A. Hagfeldt and L. Sun, *Chem. Commun.,* 2007, 3741. (b) Z. Wan, C. Jia, Y. Duan, J. Zhang, Y. Lin and Y. Shi, *Dyes and Pigments,* 2012, **94**, 150.

23 J.-L. Fillaut, J. Perruchon, P. Blanchard, J. Roncali, S. Golhen, M. Allain, A. Migalsaka-Zalas, I. V. Kityk and B. Sahraoui, *Organometallics*, 2005, **24**, 687.

24 J. Massin, L. Ducasse, T. Toupance and C. Olivier, *J. Phys. Chem. C*, 2014, **118**, 10677.

25 (a) C. Olivier, F. Sauvage, L. Ducasse, F. Castet, M. Grätzel and T. Toupance, *ChemSusChem*, 2011, **4**, 731. (b) J. Massin, L. Ducasse, M. Abbas, L. Hirsch, T. Toupance and C. Olivier, *Dyes and Pigments*, 2015, **118**, 76.

26 J. H. Delcamp, Y. Shi, J.-H. Yum, T. Sajoto, E. Dell'Orto, S. Barlow, M. K. Nazeeruddin, S. R. Marder and M. Grätzel, *Chem. Eur. J.*, 2013, **19**, 1819.

27 J.-H. Yum, T. W. Holcombe, Y. Kim, K. Rakstys, T. Moehl, J. Teuscher, J. H. Delcamp, M. K. Nazeeruddin and M. Grätzel, *Sci. Rep.*, 2013, **3**, 2446.

28 Note : under the same conditions the benchmark dye N3 afforded 9.07 % power conversion efficiency with J_{SC} = 16.71 mA cm^{-2}, V_{OC} = 755 mV and *ff* = 71.9 % (see ESI, Fig S7).

29 J. N. Clifford, E. Martinez-Ferrero, A. Viterisi and E. Palomares, *Chem. Soc. Rev.*, 2011, **40**, 1635.

30 J. Wiberg, T. Marinado, D. P. Hagberg, L. Sun, A. Hagfeldt and B. Albinsson, *J. Phys. Chem. C*, 2009, **113**, 3881.

31 B.-G. Kim, K. Chung and J. Kim, *Chem. Eur. J.,* 2013, **19**, 5220.

32 S. Haid, M. Marszalek, A. Mishra, M. Wielopolski, J. Teuscher, J.-E. Moser, R. Humphry-Baker, S. M. Zakeeruddin, M. Grätzel and P. Bäuerle, *Adv. Funct. Mater.*, 2012, **22**, 1291.

TOC entry

Tuning visible-light absorption properties of Ru-diacetylide complexes: a simple access to colorful efficient dyes for DSSC.

Samuel De Sousa, Siliu Lyu, Laurent Ducasse, Thierry Toupance* and Céline Olivier*

An attractive color palette of red, violet and blue-green chromophores was prepared for dye-sensitized solar cells application. The chromophores are used in single-dye and co-sensitized devices.